Resources, Conservation & Recycling 181 (2022) 106256

Contents lists available at ScienceDirect

Resources, Conservation & Recycling

journal homepage: www.elsevier.com/locate/resconrec

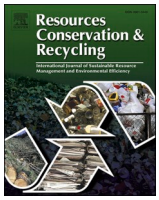

Full length article

Analysis of the kinetics, energy balance and carbon footprint of the delamination of multilayer flexible packaging films via carboxylic acids

Sibel Ügdüler [a], Tobias De Somer [a], Kevin M. Van Geem [b], Juray De Wilde [c], Martijn Roosen [a], Bram Deprez [a], Steven De Meester [a,*]

[a] Laboratory for Circular Process Engineering (LCPE), Department of Green Chemistry and Technology, Ghent University, Graaf Karel De Goedelaan 5, 8500 Kortrijk, Belgium
[b] Laboratory for Chemical Technology (LCT), Department of Materials, Textiles and Chemical Engineering, Faculty of Engineering & Architecture, Ghent University, Technologiepark 121, B-9052 Zwijnaarde, Belgium
[c] Materials and Process Engineering, Institute of Mechanics, Materials and Civil Engineering, Université Catholique de Louvain, Belgium

ARTICLE INFO

Keywords:
Delamination
Multilayer
Recycling
Circular economy
Optimization
Life cycle assessment

ABSTRACT

Flexible plastic packaging is still one of the most difficult streams to recycle due to the presence of multilayers. With multilayers being very functional during their use phase, the delamination of multilayer structures is promising because it enables the recovery of the constituent polymer layers without any degradation and/or dissolution, thus creating economic and environmental benefits. However, there is hardly any data available on the optimization of the delamination process for multilayer flexible plastic films (MFPFs), as well as the potential scale-up in terms of economic and environmental factors. Therefore, this study investigates the effect of experimental parameters such as temperature, solid/liquid (S/L) ratio, particle size, and stirring rate on the delamination rate of various MFPFs. Among these parameters, the combination of temperature and S/L ratio has the most pronounced effect on increasing the delamination rate. On the other hand, particle size does not have a significant influence on the delamination rate. Under optimal delamination conditions, more than 90% delamination is achieved in 60 min, particularly for PET-based MFPF. Simulations of the delamination process in Aspen Plus® reveal that the composition of MFPF has a significant effect on the energy consumption during the delamination process. The slower delamination kinetics of MFPFs can be compensated for through process optimization, but this typically results in higher energy requirements. The life cycle assessment (LCA) confirms that high energy consumption results in high CO_2 emissions; thus, design for MFPFs, together with process optimization, are key aspects of obtaining a competitive delamination process with economic and environmental benefits.

1. Introduction

The demand for flexible plastic packaging for use in various applications, such as food, beverage, and pharmaceuticals, continues to grow significantly due to its outstanding functional performance, including serving as an oxygen, moisture, and light barrier; printability; and food compliance (Horodytska, Valdés, & Fullana, 2018). In 2017, the worldwide production of flexible packaging was 27.4 Mt, and this value is expected to grow to 33.5 Mt by 2022 (Tiseo, 2021). These high production volumes imply that flexible plastic packaging has a high potential to contribute toward the EU recycling targets for plastics, e.g., 55% plastic recycling by 2030 (European Commission, 2018). However, the recycling rates for flexible plastic packaging are still low due to the lack of infrastructure for the collection and advanced sorting for flexibles, as well as their inherently complex structures, including the presence of multilayers (CEFLEX, 2021). Plastic packaging can be made of one polymer or a combination of polymers, each with its own specific functionality. Developing tailored packaging films results in superior preservation performance for the products embedded in the packaging, such as food. However, their complexity, especially the presence of multilayer structures, impedes recycling because they cause incompatibility issues during mechanical recycling, for example, between polyolefins and heteropolymers (Schyns & Shaver, 2020). Therefore, flexible plastic packaging is still mainly incinerated or landfilled to date,

* Corresponding author.
E-mail address: Steven.DeMeester@UGent.be (S. De Meester).

https://doi.org/10.1016/j.resconrec.2022.106256
Received 3 December 2021; Received in revised form 18 February 2022; Accepted 20 February 2022
Available online 5 March 2022

Table 1
The tested multilayer flexible packaging films (MFPFs) and their respective composition.

Sample code	Layer 1	Layer 2	Layer 3	Layer 4	Layer 5
A	Corona PET	PVB-color and PVC white inks	SF-PU adhesive	Transparent PE	
B	Two-component (2 K)-matt lacquer	ChemPET	NC and PU white inks	SB-PU adhesive	Transparent PE
C	OPP	NC-magenta	SF-PU adhesive	Transparent PE	
D	MOPE	SB-PU adhesive	Transparent PE		

creating both economic and environmental concerns (Kaiser, Schmid, & Schlummer, 2018).

In order to increase the recycling rate for plastic packaging, handling these multilayer plastics is gaining more and more interest from industry and research. One of the methods of enabling the separation of different components in multilayer structures is selective dissolution. In this process, the solvent and process conditions are chosen selectively so that only the target polymer is dissolved and all the other undissolved components can be removed from the solution by means of solid/liquid separation techniques (Niaounakis, 2019). Selective dissolution has already been applied to multilayer flexible plastic films (MFPF) containing polyolefins because their polarity is quite different than that of heteropolymers such as polyethylene terephthalate (PET), polyamide (PA), and polyvinylchloride (PVC) (Kippenhahn et al., 2003 Lindner, 2000; Lynch & Nauman, 1994; Thome, Kraus, & Schubert, 1993;). These kinds of processes have also been applied at an industrial scale by APK AG through the Newcycling® process, in which PA/PE multilayer films are separated via selective PE dissolution at a scale of 8 kt/year (Coperion, 2020). Selective dissolution results in high-quality recyclates; however, the selection of a suitable solvent, the need for the addition of large amounts of anti-solvent for efficient precipitation, and also the drying of the recovered polymers are drawbacks of this process (Kaiser et al., 2018 Mumladze et al., 2018;). In order to prevent the use of large amounts of anti-solvent, the selective decomposition of polymer layers can be an option for separating MFPFs. For example, in the method introduced by Patel et al., sulfuric acid was used to degrade PET selectively for the separation of the PET/PE multilayer structure (Patel, Patel, & Vaviya, 2016). Similarly, Kulkarni et al. used a sub- and supercritical water process to depolymerize the PET and PA layers of aluminum-containing MFPF (Kulkarni, Daneshvarhosseini, & Yoshida, 2011). Although the selective decomposition of constituent polymer layers is promising in terms of polyolefin recovery and decreased solvent consumption, medium (solvent and potential degraded components) recovery is challenging (Ügdüler et al., 2020).

Another possibility is separating the different layers of a multilayer structure, generally referred as “delamination,” which can be induced via the reaction/dissolution of the tie layers used to laminate dissimilar polymer layers. Various solvents and acids have been studied to investigate their delamination performance. For example, Mumladze et al. used switchable hydrophilicity solvents (SHSs) to break the chemical and mechanical bonds between multilayer flexible packaging waste, thus allowing the separation of the layers individually (Mumladze et al., 2018). Similarly, in various patents, inorganic acids, such as nitric acid and phosphoric acid, are used for the delamination of Al-containing composite packaging or industrial refuse (Bing, 2012 Huang & Shao, 2002; Mukhopadhyay, 2001;). Industrially applied delamination technologies have mainly focused on used beverage cartons (UBCs), commonly referred to as Tetra Pak® recycling. For instance, in China, various companies are performing acid-based delamination of PE/Al multilayer structures in the presence of formic acid (Zawadiak, 2017). Likewise, Saperatec GmbH (Germany) uses a patented method based on the usage of a micro-emulsion comprised of swelling agents, carboxylic acids, water, and surfactants for the delamination of multilayer packaging containing aluminum. These micro-emulsions reduce interfacial tensions, enabling the penetration of the interphase and counteracting the adhesion of the multilayers (Lovis, Seibt, & Kernbaum, 2015).

Among the various separation methods for multilayer structures, delamination through the dissolution of tie layers is promising because it only degrades or dissolves the smallest part of the solids, that is, the resins used in the tie layers. Delamination efficiency is mainly dependent on the diffusion and dissolution power of the reagent. Delamination can be seen as a consecutive three-stage process: a period of reagent diffusion through the polymer layers, the dissolution of the adhesive layer, and, finally, the disconnection of the polymer layers from one another, indicating complete delamination (Ügdüler et al., 2021). The selection of the delaminating reagent is also crucial in obtaining an efficient delamination. It has been shown that, as compared to organic solvents, carboxylic acids can delaminate a broader range of multilayer structures (Lovis et al., 2015 Massura, Marçal De Souza, & Crochemore, 2002; Schulze, 2018; Sobek, Polak, & Hajek, 2015; Xianghui, 2007;). Shorter chain carboxylic acids are also more effective delamination media because they diffuse more quickly through the polymer layers (Hamilton, 1999). This has also been proven in a previous study by using a permeation unit used to test the diffusivity levels of carboxylic acids (Ügdüler et al., 2021). It has been observed that the diffusion of formic acid through a PET layer is more than 20 times faster as compared to the diffusion of decanoic acid (Ügdüler et al., 2021). Similarly, among the tested carboxylic acids, the fastest dissolution of polyurethane (PU)-based adhesives was obtained with formic acid, followed by acetic acid and hexanoic acid, respectively (Ügdüler et al., 2021).

Whereas formic acid is identified as an optimal reagent, there is no systematic scientific study that describes the optimal delamination conditions for various MFPFs in the presence of formic acid. Moreover, there are hardly any data available to show the scale-up potential of the delamination of MFPFs in terms of economic and environmental aspects. Therefore, with this study, we aim to accomplish the following:

- To investigate the effect of various experimental conditions, such as temperature, solid/liquid (S/L) ratio, particle size and stirring rate, on the delamination rate of diverse MFPFs;
- To determine optimal delamination conditions for different MFPFs based on the experimental kinetic studies performed according to the design of experiments (DoE);
- To develop a more thorough understanding of the mass and energy balance and environmental performance of the delamination process through Aspen Plus® simulations performed based on the best-fit kinetic model, combined with life cycle assessment (LCA).

2. Materials and method

2.1. Multilayer samples, chemicals, and reagents

Various MFPFs with different compositions, given in Table 1, and the cured aromatic solvent-based (SB)-PU and solvent free (SF)-PU adhesives were supplied by Siegwerk Druckfarben AG & Co. These types of multilayer samples are used for various packaging applications, such as food, labels, and hygiene products (Nowofol, 2021). Samples A and B contain corona-treated PET films (corona PET) and chemically treated PET films (chemPET), respectively. Compared to untreated PET films, corona PET and chemPET are more suitable for the packaging industry

Table 2
Calculation of the coded values for each variable for the generation of a quadratic equation.

Variable	Equation	Unit of each parameter used in the equation
Stirring rate (X_1)	$X_1 = (rpm - 450)/75$	rpm
Temperature (X_2)	$X_2 = (T - 348.15)/12.5$	K
S/L ratio (X_3)	$X_3 = (S/L - 0.004)/0.0015$	g/mL
Particle size (X_4)	$X_4 = (Part.\ size - 11)/4.5$	mm

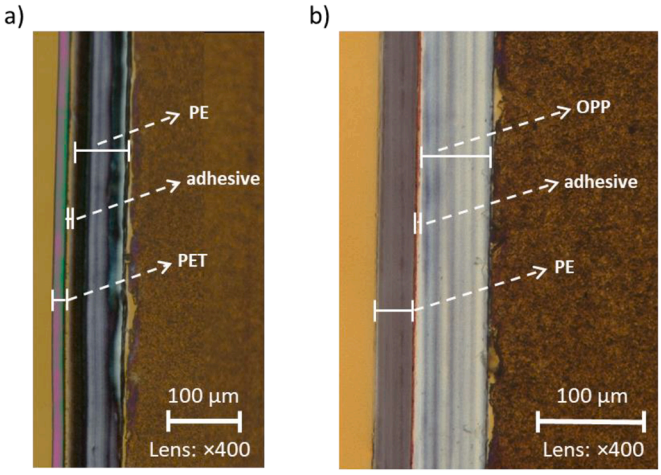

Fig. 1. POM images of a) sample A and b) sample C.

because they provide better adhesion for coatings or printing inks due to increased surface energy (Addev Materials, 2021). Samples C and D contain oriented polypropylene (OPP) and machine direction-oriented polyethylene (MOPE), respectively. These oriented polymer films provide higher transparency, better rigidity, and improved barrier properties as compared to non-oriented polymer films (Plastemart, 2020). In the kinetic studies, these MFPFs were reduced in size as defined by the DoE: 2 × 2 mm, 6.5 × 6.5 mm, 11 × 11 mm, 15.5 × 15.5 mm and 20 × 20 mm. Formic acid (≥98%) was supplied by Sigma Aldrich (Merck).

2.2. Experimental kinetic studies on MFPFs

Kinetic studies were performed on the delamination of each MFPF under different experimental conditions, as defined by central composite inscribed design (CCI). This DoE was constructed based on four factors, namely temperature, stirring rate, S/L ratio, and particle size, as shown in Section 3.1 (Table 5). The limits of each factor were determined through exploratory experiments, where a significant change in the delamination rate of MFPFs is observed. For the boundaries of S/L ratio, the maximum solubility of each PU adhesive in formic acid has been considered (Appendix, Fig. A-1). The experiments for the kinetic study were carried out in a round-bottom flask equipped with a condenser and an agitator for stirring. The 100 mL flask containing formic acid was placed into a thermal bath at room temperature (RT) and preheated to the target temperature based on DoE prior to the addition of MFPF in order to minimize the delays prior to reaching the specified temperature at atmospheric pressure. During the 90 min of reaction, a 2 mL aliquot of liquid sample was collected from the delamination solution (50 mL) at every time interval (every min during the first 5 min of delamination, followed by 5, 10 and 20 min intervals). The collected sample was then transferred into a vial and immersed in an ice bath to interrupt the dissolution of the (PU) adhesive. Afterward, these collected samples were analyzed via UV-VIS measurements. Based on the calibration curves elaborated for each pure cured PU adhesive in formic acid, the amount of adhesive dissolved during the delamination of the MFPFs was quantified.

The optimal delamination conditions were determined based on the results of the kinetic experiments. The concentration of the adhesive in formic acid after 60 min of reaction time was taken as a reference for comparing the experimental conditions. Because a higher concentration of the adhesive indicates higher delamination %, the conditions under which the adhesive concentration were maximized were considered in determining the optimal conditions for each MFPF. Firstly, the experimental datasets were analyzed to determine the outliers using the residual plots generated by the plot function in R software. The resulting datasets were then used in establishing the quadratic model with which to describe the relationship between the experimental factors (temperature, stirring rate, S/L ratio, and particle size) and the adhesive concentration after 60 min. While constructing the quadratic model (Eq. (1)), the non-significant terms ($p > 0.05$) were removed incrementally, and this was repeated until the quadratic model with the highest adjusted R^2 was obtained. This was performed by means of the Response Surface Methodology (RSM) package in the R environment.

$$Y = \beta_0 + \sum_{i=1}^{p} \beta_i x_i + \sum_{i=1}^{p} \sum_{j=1}^{p} \beta_{ij} x_i x_j + \sum_{i=1}^{p} \beta_{ii} x_i^2 \quad (1)$$

where Y is the response (adhesive concentration (g/mL), β_0 is the overall mean response, X_i and X_j refer to the i^{th} and j^{th} factor of the DoE, and β_i, β_{ij}, and β_{ii} refer to the coefficients describing the main effects for each factor, the two-way interaction between the i^{th} and j^{th} factors, and the quadratic effect for the i^{th} factor, respectively.

In order to generate a quadratic equation for each MFPF, the experimental variables were converted to their coded values by considering the mean value of the variable range (numerator) and the distance between the center points of the DoE (denominator), as given in Table 2.

2.3. Analytical techniques for the quantification of the adhesives (PU) in the acid medium

The medium containing the dissolved PU adhesive and formic acid was analyzed via UV/Vis spectroscopy on a UV-1280 multipurpose UV/Vis spectrophotometer with a scan range of 190–1100 nm. The collected 2 mL aliquots were transferred into a semi-micro quartz cuvette with an outer cell dimension of 12.5 mm × 12.5 mm × 45 mm and an optical pathlength of 10 mm. Pure formic acid solutions were measured as a reference. For each sample, the optical spectrum measurements were repeated three times to ensure their consistency and repeatability. During the spectrum scan, the strongest absorption was recorded at 256 nm for both SB-PU and SF-PU adhesives because they are aromatic-based polyurethanes (Zhou, Wu, Xiong, He, & Chen, 2004). Based on the Beer-Lambert law (Beer, 1852), calibration curves were elaborated for each type of PU adhesive by using known concentrations (Appendix, Fig. A-2). These curves were used to calculate the concentration of dissolved adhesive during the experimental delamination kinetic study. Similarly, the solubility of both adhesives in formic acid was measured by UV/Vis spectroscopy in the temperature range of 25–95°C (Appendix, Fig. A-1).

2.4. Characterization of the composition of MFPFs

The composition of the MFPFs and the thickness of each polymer and adhesive layer were determined by making microtome cuts of 100 µm from the lateral section of the plastic film using a Leica RM 2245 microtome. These cuts were placed on Canada balsam-containing glass microscope slides and kept under a bench press for 48 hrs. The samples were thereafter analyzed using polarized optical microscopy (POM) on a Keyence VHX-500F microscope. Because different types of polymers

Table 3
Kinetic models and their associated equation applied in this study.

Kinetic models	Equation
Continuous logistic equation or Verhulst equation	$\frac{d[PU_L]}{dt} = k * [PU_L] * \left(1 - \frac{[PU_L]}{[PU_L]_{eq}}\right)$
Richards growth equation	$\frac{d[PU_L]}{dt} = k_1 * [PU_L] * \left(1 - \left(\frac{[PU_L]}{[PU_L]_{eq}}\right)^{k_2}\right)$
Hyper-logistic function	$\frac{d[PU_L]}{dt} = k_1 * [PU_L]^{k_2} * \left(1 - \frac{[PU_L]}{[PU_L]_{eq}}\right)^{k_3}$
Adjusted Blumberg model	$\frac{d[PU_L]}{dt} = k_1 * [PU_L]^{k_2} * \left(1 - \frac{[PU_L]}{[PU_L]_{eq}}\right)$
WEP-modified logistic growth model	$\frac{d[PU_L]}{dt} = (k_1 + k_2 * [PU_L]) * \left(1 - \frac{[PU_L]}{[PU_L]_{eq}}\right)$

show different colors under optical light, the thicknesses of different polymers and adhesives could be detected easily. The PU adhesives were visible in the microtome section as a thin layer, 3 μm in thickness, between the polymer layers, as shown in Fig. 1.

The density of both cured SB-PU and SF-PU adhesives was measured as 1.1 g/cm^3 via a density scale on a Kern EMB-V. Based on POM and density measurements, the mass of the adhesive layer per cm^2 surface area of MFPF samples was calculated as 0.00033 g/cm^2, and it is assumed that the adhesive is homogenously distributed over the polymer surface. The delamination % of MFPFs was expressed in terms of the mass of dissolved adhesive, which was calculated via the following equations:

$$M_A = \frac{M_{Total}}{M_{MFPF}} \times 0.00033\left(\frac{g}{cm^2}\right) \times A \tag{2}$$

$$Dissolved\ adhesive\ (\%) = \frac{M_t}{M_A} \times 100 \tag{3}$$

where M_A is the total mass of adhesive present in the MFPF (g), M_{Total} is the total mass of MFPF used for the delamination experiment (g), M_{MFPF} is the mass of one MFPF particle (g), A is the surface area of one MFPF particle (cm^2), and M_t is the mass of adhesive dissolved in the acid medium at a specific time during kinetic studies (g).

2.5. Simulation of delamination process in Aspen Plus®

2.5.1. Best-fit kinetic model

The delamination kinetics of the multilayer samples in the reactor were defined through the best-fit kinetic model. As presented in our previous study (Ügdüler et al., 2021), the delamination kinetics of the MFPFs can be described fundamentally based on diffusivity and solubility phenomena. Because the dissolution of the adhesive begins upon the diffusion of formic acid to the adhesive layer, a small lag time is observed before the increase in adhesive concentration at the beginning of the reaction. Because the increase in the PU adhesive concentration indicates the delamination of the multilayer sample, the dissolution rates of the adhesives were calculated via first-order dissolution kinetics using the following equation:

$$R_{diss} = \frac{d[PU_L]}{dt} = k_r * \left(1 - \frac{[PU_L]}{[PU_L]_{eq}}\right) \tag{4}$$

where R_{diss} is the dissolution rate of the adhesive (mg/(L.s)), k_r is the dissolution rate constant (mg/(L.s)), and $[PU_L]$ and $[PU_L]_{eq}$ are the concentration of PU adhesive in the delamination solution and the maximum solubility of PU (mg/L), respectively.

The maximum solubility of PU adhesives, $[PU_L]_{eq}$, was derived based on the experimental solubility data of each adhesive (Fig. A-1). Because it is assumed that the accumulated acid between the polymer layers is concentrated before the disconnection of the layers, the $[PU_L]_{eq}$ value only changes based on the temperature. The correlation between the temperature (in K) and the maximal solubility of each adhesive (SB-PU and SF-PU) (mg/mL) in the acid medium was described by a polynomial equation as follows (Ügdüler et al., 2021):

$$[PU_L]_{eq,SB-PU} = 3.530864 * 10^{-6} * T^4 - 4.495106 * 10^{-3} * T^3 + 2.136904 * T^2 - 4.492899 * 10^2 * T + 3.523230 * 10^4 \tag{5}$$

$$[PU_L]_{eq,SF-PU} = 2.494265 * 10^{-7} * T^3 - 2.469980\text{E} * 10^{-4} * T^2 + 8.167356 * 10^{-2} * T - 8.310889 \tag{6}$$

Based on these considerations, five kinetic models were tested (Verhulst equation, Richards growth equation, Hyper logistic function, Adjusted Blumberg model and WEP-modified logistic growth model) that consider potential lag time due to the diffusion and also the saturation of the liquid medium in order to define the delamination kinetics in the reactor (Table 3).

One of the tested kinetic models is the continuous logistic equation or Verhulst equation, which describes the growth of a population in a habitat of finite resources (Ji, 2013). It was also reported that this logistic equation is described by a first-order ordinary differential equation (Sweilam, Khader, & Mahdy, 2012). In this model, the growth rate begins exponentially but then decreases to zero as the q approaches the limit q_e, resulting in a sigmoidal growth trajectory (Ji, 2013). Similar to the Verhulst equation, the Richards growth equation also exhibits sigmoidal growth, but it extends the growth equation to fit the empirical data (Tsoularis & Wallace, 2002). The hyper logistic function is another logistic equation based on a modification of the Verhulst logistic growth in which the inflexibility of the inflection point is eliminated (Tsoularis & Wallace, 2002). The adjusted Blumberg model is the simplified version of the hyper-logistic function (Zeide, 1993). The WEP-modified logistic model is also a modified standard logistic model, which consists of the terms representing a constant and proportional growth rate (Tsoularis & Wallace, 2002).

These empirical kinetic models were fitted to the experimental data (the concentration of the adhesive [mg/L] as a function of time[s]) using an R script. For the parameter regression in R, the FME package and the ModFit function with the pseudorandom-search algorithm as the solver were used.

In order to determine the best-fit model via which to describe the delamination kinetics of MFPFs, error analysis of the applied models in terms of the experimental data was performed using various validation techniques, i.e., the sum of square of errors (SSE), the hybrid fractional error function (HYBRID), Theil's inequality coefficient (TIC), and the nonlinear Chi-square test (χ^2), as given in Eq. (7), (8), (9), and (10). The average results of these statistical tests are presented in Table A-1. Because the considered kinetic models are not defined by default in Aspen Plus®, the best-fit model was implemented by means of a FORTRAN script, as shown in the methodology of Pirro et al. (2020).

$$SSE = \sum_{i=1}^{n} (x_{calc} - x_{meas})_i^2 \tag{7}$$

$$HYBRID = \frac{100}{n-p} \sum_{i=1}^{n} \left[\frac{(x_{meas} - x_{calc})^2}{x_{meas}}\right]_i \tag{8}$$

Table 4
Overview of the various steps and process settings considered for the recovery of delaminated plastic films.

Unit operation	Sample A	Sample D	Comment
Plastic load (kg/h)	1000	1000	In CSTR reactors at the maximum capacity of 100 m^3
No of reactors for delamination	5	10	10 reactors for sample D due to • The lower solubility of SF-PU • Slower delamination kinetics related to the sample composition
Flash column	Only at the end of the delamination process	After each reactor	For sample D, acid is evaporated until 97.5% in a flash column after each reactor, condensed, and then sent to the next reactor
Flash dryer	11.5 w% acid residue on the delaminated plastic surface is decreased to 5 w% (Larrain et al., 2021)		$E_{flash\ drying} = \frac{(C*(T_o - T_i) + \Delta H_v)*\dot{M}*(wM_i - wM_o)}{\eta_{dryer}}$ where $E_{flash\ drying}$ is the energy consumption of the flash dryer (kW), C is the heat capacity of formic acid (kJ/kg.K), and T_i and T_o are the input and output temperatures of the flash dryer (K), respectively. ΔH_v is the heat of evaporation (kJ/kg), $\dot{M}$ is the mass flow (kg), and wM_i and wM_o are the moisture content before and after drying (kg), respectively. Finally, η_{Dryer} is the efficiency of the dryer (49%) (Larrain et al., 2021).
Neutralization	Neutralization of the remaining 5 w% acid with a 35 w% hydrated lime ($Ca(OH)_2$) solution (National Lime Association, 2000).		$2HCOOH + Ca(OH)_2 \rightarrow (HCOO)_2Ca + 2H_2O$ To simulate the neutralization, a RSTOIC block was used, where the $Ca(OH)_2$ supply was set as such that the residual formic flow is 0 kg/h in the output.
Mechanical dryer	Drying of samples after neutralization		The energy consumption of the mechanical dryer is taken as 90 kW for the processing of 1 ton/h of plastic films (Herbold, 2016)
Thermal dryer	The 11.5 w% water moisture on the plastic surface is reduced to 0.5 w%		$E_{thermal\ drying} = \frac{(C*(T_o - T_i) + \Delta H_v)*\dot{M}*(wM_i - wM_o)}{\eta_{dryer}}$ where $E_{flash\ drying}$ is the energy consumption of the flash dryer (kW), C is the heat capacity of formic acid (kJ/kg.K), and T_i and T_o are the input and output temperatures of the flash dryer (K), respectively. ΔH_v is the heat of evaporation (kJ/kg), $\dot{M}$ is the mass flow (kg), and wM_i and wM_o are the moisture content before and after drying (kg), respectively. Finally, η_{Dryer} is the efficiency of the dryer (49%) (Larrain et al., 2021).

$$TIC = \frac{\sqrt{\sum_i (x_{calc} - x_{meas})^2}}{\sqrt{\sum_i {x_{calc}}^2} + \sqrt{\sum_i {x_{meas}}^2}} \quad (9)$$

$$\chi^2 = \sum_{i=1}^{n} \frac{(x_{calc} - x_{meas})^2}{x_{meas}} \quad (10)$$

where x_{calc} and x_{meas} are the experimental and calculated values, respectively, for the concentration of PU adhesive in the delamination solution $[PU_L]$ (mg/L). The subscript i refers to the value associated with the i^{th} component, n is the number of data points, and p is the number of parameters in the model.

2.5.2. Downstream of the Aspen Plus® simulations

The best-fit kinetic model of the delamination kinetics has been used to determine the mass and energy balances of the delamination process via Aspen Plus® simulations. In order to investigate the effect of MFPF composition, process schemes were performed at a capacity of 1000 kg/h plastic for both sample A (PET-based MFPF) and sample D (PE-based MFPF), which were laminated with SF-PU and SB-PU adhesive, respectively, as given in Table 1. In the process, the plastics and the acid were mixed and fed into a series of co-current CSTR reactors (each with a maximum volume of 100 m^3). The fed acid undergoes a post-treatment before recirculation in order to prevent the saturation of the medium in the reactors. The optimal reactor conditions were set based on the highest experimental average concentration of dissolved adhesive after 60 minutes of reaction time (at 87.5°C, 525 rpm stirring rate, 0.0055 g/mL S/L ratio, and 6.5 mm of particle size). The residence time in the reactors was adjusted in such a manner that maximum adhesive dissolution could be achieved under these defined reactor conditions. In the simulations of Sample A, five reactor series were used to achieve 95% adhesive dissolution. On the other hand, in the simulations of Sample D, ten reactors were considered in order to increase its delamination yield. Because the solubility of the SF-PU adhesive (0.00073 g/mL at 95°C) in sample D is lower, for sample D, the acid was regenerated after each reactor and sent to the next reactor. In this way, the concentration of the adhesive in the medium was reduced, thus limiting the fast saturation of the acid medium. However, even after passing through ten reactors in series, with intermediate acid purification, only a 58% delamination of Sample D could be obtained due to its slow delamination kinetics. Regarding the flow of delaminated plastic films, it is believed that 11.5 w% acid residue is present on the surface of delaminated plastic films after they are sieved from the acid medium when leaving the final reactor (Larrain et al., 2021). Therefore, the delaminated plastic films were fed into a flash dryer to reduce the amount of acid on the surface of a plastic film below 5 w%. After the flash dryer, the remaining formic acid on the plastic film surface was neutralized with a 35 w% hydrated lime ($Ca(OH)_2$) solution, which is typically used in industry for the neutralization of acidic waste streams (National Lime Association, 2000). For the simulation of the neutralization, a RSTOIC block was used, in which the $Ca(OH)_2$ supply was set so that the residual formic acid flow was non-existent in the output. The heat released in the neutralization step was transferred to the flasher by means of a heat-recovery cycle. The final drying of the plastic films consists of two steps, namely a mechanical drying step, followed by a thermal drying step. After mechanical drying, the plastics are assumed to have a residual moisture content of 11.5 w%, and this amount is decreased to 0.5 w% after thermal drying (Larrain et al., 2021). The energy consumption of the mechanical dryer is taken as 90 kW for processing of 1 ton/h of plastic films (Herbold, 2016). Each step of the delamination process toward the recovery of the delaminated plastic films of Sample A and Sample D is summarized in Table 4.

After the separation of the delaminated plastics from the medium, the liquid phase is sent to a flash drum under a vacuum to recover the acid as a pure vapor phase. The pressure and temperature in the flash drum are optimized so as to minimize the total energy consumption, resulting in lower CO_2 emissions. Afterward, the vapor phase is compressed using a compressor with an efficiency of 72%, set via Aspen Plus®, and recirculated. During the simulations, the energy consumption of the process was optimized based on the 97.5 v% recovery of the feed in the flash drum. Afterward, a sensitivity test was performed, in which the recovery of the acid vapor in the final flash drum was varied between 90% and 100%.

Because the solubility of the adhesives in formic acid is quite low, as shown in Fig. A-1, it is assumed that such low concentrations would not affect the vapor pressure of the mixture significantly (Bawn, Freeman, & Kamaliddin, 1950 Bercea, Eckelt, & Wolf, 2009; Noda, Higo, Ueno, & Fujimoto, 1984; Rathbone, Haynes, Blanch, & Prausnitz, 1990; Sadeghi & Shahebrahimi, 2011; Sakurada, Nakajima, & Fujiwara, 1959; Sheehan & Bisio, 1966;). Therefore, the influence of the dissolved adhesives on the vapor pressure of the formic acid was neglected during the simulations.

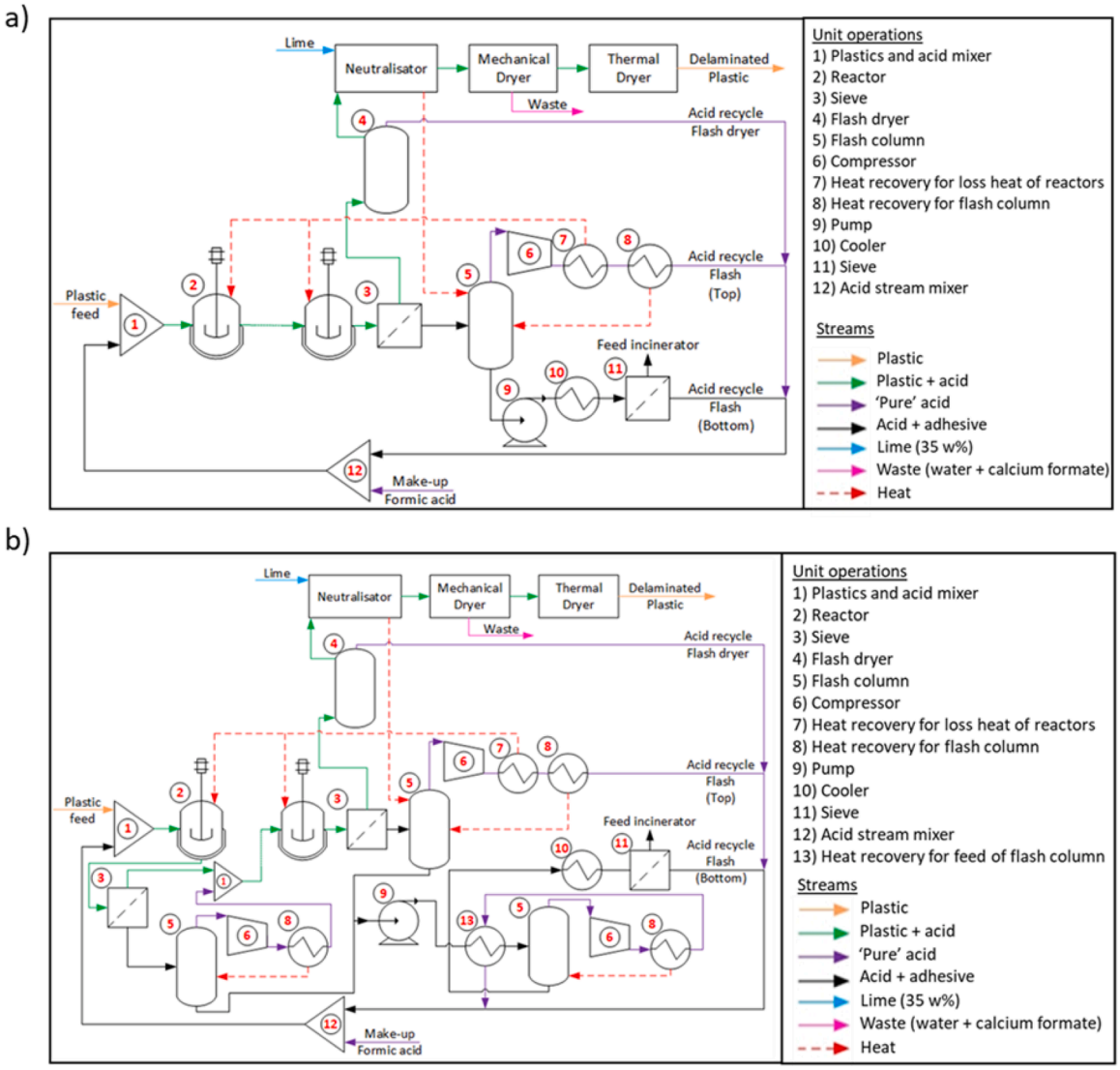

Fig. 2. Aspen Plus® process flow diagram of delamination medium recirculation for a) sample A and b) sample D.

Due to the evaporation of the acid, the bottom fraction of the flash drum will be upconcentrated, which may cause the precipitation of the dissolved adhesives. Therefore, the bottom fraction of the flash drum is further purified by cooling down the flow (35°C) to precipitate the adhesives. The adhesives are then removed from the bottom fraction by means of a sieve/membrane, and the liquid phase is recirculated, together –with the pure evaporated media. At this point, different acid evaporation ratios (90–100%) are considered. The acid evaporation ratio indicates the amount of acid evaporated in the final flash unit after the delamination process divided by the total amount of acid sent to the flash unit. The remainder of the acid in the flash unit is still recirculated in the system but without evaporation. Because all of used acid is recirculated, the total acid consumption does not change depending on the acid evaporation ratio. Even though the non-evaporated acid ratio includes dissolved adhesives, during its recirculation, the delamination kinetics are not affected in the tested range (90–100% acid evaporation ratio), because the solubility of the adhesives is quite low.

The process flow diagrams of delamination medium recirculation for both MFPF samples are given in Fig. 2.

As a final step in the simulations, the energy consumption to heat and cool the flows was minimized by introducing heat exchangers into the process by performing a pinch analysis. Accordingly, the hot recycle stream was used to cover the heat losses of the reactors and warm up the fresh feed. The residual heat from this stream was used for heating up the flash vessel. Therefore, the net heat consumption of the flash drum is zero for both samples. The heat and energy consumption values in each process step at different acid evaporation ratios in the (final) flash unit (%) are given in Table 8.

2.6. Methodology for the LCA

An LCA was performed based on the mass and energy balances obtained on the Aspen simulations of Samples A and D, which were laminated with SF-PU and SB-PU adhesive, respectively. Because the entire recycling process of multilayer samples was taken into account in the LCA, the calculations were performed by considering a foreground and background system, as elaborated in the Appendix, in Fig. A-3. The foreground system corresponds to all processes related to the delamination flow schemes, as presented in Fig. 2. The carbon footprint for the inputs/outputs in the foreground system were extracted from the Ecoinvent Database v3.1 in OpenLCA 1.9. The background system consists of the processes that are outside of the foreground system, e.g., shredding, washing, and extrusion. For the background system, the data were adopted from the literature (Civancik-Uslu et al., 2021). For example, during the initial washing step, before delamination, to remove any remaining dust/grease/food from the MFPF waste, a loss of

Table 5
Central composite inscribed experimental design (CCI) was used to determine optimal delamination conditions.

Exp. no	Process conditions				Dissolved adhesive at 60 min (%)			
	Temp. (°C)	Stirring rate(rpm)	S/L ratio(g/mL)	Particlesize(mm)	Sample A	SampleB	SampleC	Sample D
1	62.5	375	0.0025	15.5	27.15	21.18	11.25	2.59
2	2.5	375	0.0055	6.5	30.11	19.02	10.38	5.13
3	62.5	525	0.0025	6.5	35.98	20.33	36.17	9.47
4	62.5	525	0.0055	15.5	33.18	8.39	16.91	5.26
5	87.5	375	0.0025	6.5	40.88	77.99	16.69	11.30
6	87.5	375	0.0055	15.5	75.57	37.62	13.95	6.26
7	87.5	525	0.0025	15.5	66.17	38.39	13.90	6.57
8	87.5	525	0.0055	6.5	85.01	53.02	21.03	11.14
9	75	450	0.004	11	44.47	48.71	14.58	4.57
10	75	450	0.004	11	44.31	26.67	5.70	8.71
11	62.5	375	0.0025	6.5	21.21	18.50	2.76	2.22
12	62.5	375	0.0055	15.5	16.16	18.44	6.36	2.52
13	62.5	525	0.0025	15.5	16.66	25.57	51.21	12.40
14	62.5	525	0.0055	6.5	21.65	19.19	18.75	12.02
15	87.5	375	0.0025	15.5	41.76	33.23	4.54	5.21
16	87.5	375	0.0055	6.5	33.02	44.46	9.64	13.58
17	87.5	525	0.0025	6.5	28.95	41.54	13.55	5.66
18	87.5	525	0.0055	15.5	47.60	69.82	16.15	5.17
19	75	450	0.004	11	75.43	32.56	9.76	3.14
20	75	450	0.004	11	56.82	32.63	21.43	8.89
21	50	450	0.004	11	20.05	25.30	3.61	2.44
22	100	450	0.004	11	72.40	22.54	8.05	58.52
23	75	300	0.004	11	46.07	73.51	6.16	11.05
24	75	600	0.004	11	77.36	34.95	14.80	8.37
25	75	450	0.001	11	36.24	27.50	98.00	8.73
26	75	450	0.007	11	41.96	16.85	9.23	7.18
27	75	450	0.004	2	20.99	21.94	70.40	11.86
28	75	450	0.004	20	24.96	35.46	13.02	7.98
29	75	450	0.004	11	55.56	46.33	25.44	6.75
30	75	450	0.004	11	84.52	51.40	27.08	12.54

18.8 w% of the waste was considered (Civancik-Uslu, Puig, Hauschild, & Fullana-i-Palmer, 2019). Afterward, the generated wastewater was treated by using chemicals such as $FeCI_3$, NaOH, and polyelectrolyte. For the delamination process, the energy and product consumption values obtained through Aspen Plus® simulations at a 95% acid evaporation ratio were considered because the total energy consumptions at different acid evaporation ratios were similar based on the sensitivity analysis, as will be discussed in Section 3.2.2. After the delamination process, the separated types of plastic film, e.g., PET and PE, were recovered via a sink-float step. Subsequently, the monolayer films were directly extruded from flakes without prior regranulation.

In the analyzed processes, an input of 1000 kg post-consumer MFPF waste was considered as a functional unit. The results of the LCA have been expressed in terms of carbon dioxide equivalent emission (CO_2-eq) per kg of MFPF waste via the ReCiPE (H) Midpoints impact assessment method. The impact of the delamination processes is compared to a reference scenario in which the multilayer plastic materials would be incinerated, with energy recovery, and the produced recyclates would substitute for virgin polymers. Based on all these considerations, the total carbon footprint of the entire process is calculated using the carbon footprint values of each step of the delamination process at a 95% acid evaporation ratio (Table A-4).

3. Results and discussion

3.1. Effect of the experimental parameters on delamination rate

Based on the DoE, kinetic studies were performed for each MFPF in order to investigate the effect of process conditions (temperature, stirring rate, S/L ratio, and particle size) on the delamination rate and also optimal delamination condition per type of MFPF Table 5). The amount of dissolved adhesive in the medium after 60 minutes of reaction time was taken as a reference for each sample under each experimental condition. According to the results, the highest average adhesive concentration was obtained under the conditions of Experiment 8 (at 87.5°C, 525 rpm, 0.0055 g/mL S/L ratio, and 6.5 mm particle size). On the other hand, the lowest average adhesive concentration was observed under the conditions of Experiment 11 (at 62.5°C, 375 rpm, 0.0025 g/mL S/L ratio, and 6.5 mm particle size). When analyzing the dissolved adhesive of each MFPF separately, the conditions under which the maximum adhesive concentration was obtained varied with the MFPFs. This is due to the compositional difference between MFPFs, which affected the interaction of the parameters in different ways. Therefore, the relationship between experimental parameters was described for each MFPF through Response Surface Methodology (RSM), as given in Eq. (11), ((12), (13), and (14) for Samples A, B, C, and D, respectively. In these equations, the adhesive concentration after 60 min of reaction time (mg/L) was taken as an output, and x_1, x_2, x_3, and x_4 refer to the coded values of stirring rate, temperature, S/L ratio, and particle size, respectively, calculated as shown in Table 2.

$$Conc\left(\frac{mg}{L}\right)_A = 92.5929 + 2.7997 * x_1 + 24.9087 * x_2 + 28.0337 * x_3 + 17.6755 * x_2 * x_3 - 6.4928 * x_2^2 - 6.1803 * x_3^2 - 14.9303 * x_4^2 \quad (11)$$

$$Conc\left(\frac{mg}{L}\right)_B = 29.37603 + 1.07610 * x_1 + 10.81894 * x_2 + 9.19818 * x_3 - 0.70776 * x_4 + 2.91096 * x_1 * x_2 + 1.55822 * x_1 * x_3 + 1.33562 * x_1 * x_4 + 5.44521 * x_2 * x_3 + 3.57321 * x_2^2 - 10.16823 * x_3^2 + 0.83795 * x_4^2 \quad (12)$$

$$Conc\left(\frac{mg}{L}\right)_C = 33.125 + 6.0812 * x_1 - 1.523 * x_2 + 5.8405 * x_3 - 4.4343 * x_1 * x_2 + 2.9095 * x_2 * x_3 + 1.972 * x_2 * x_4 - 4.8438 * x_1^2 - 6.25 * x_2^2 - 20.0593 * x_3^2 + 20.7812 * x_4^2. \quad (13)$$

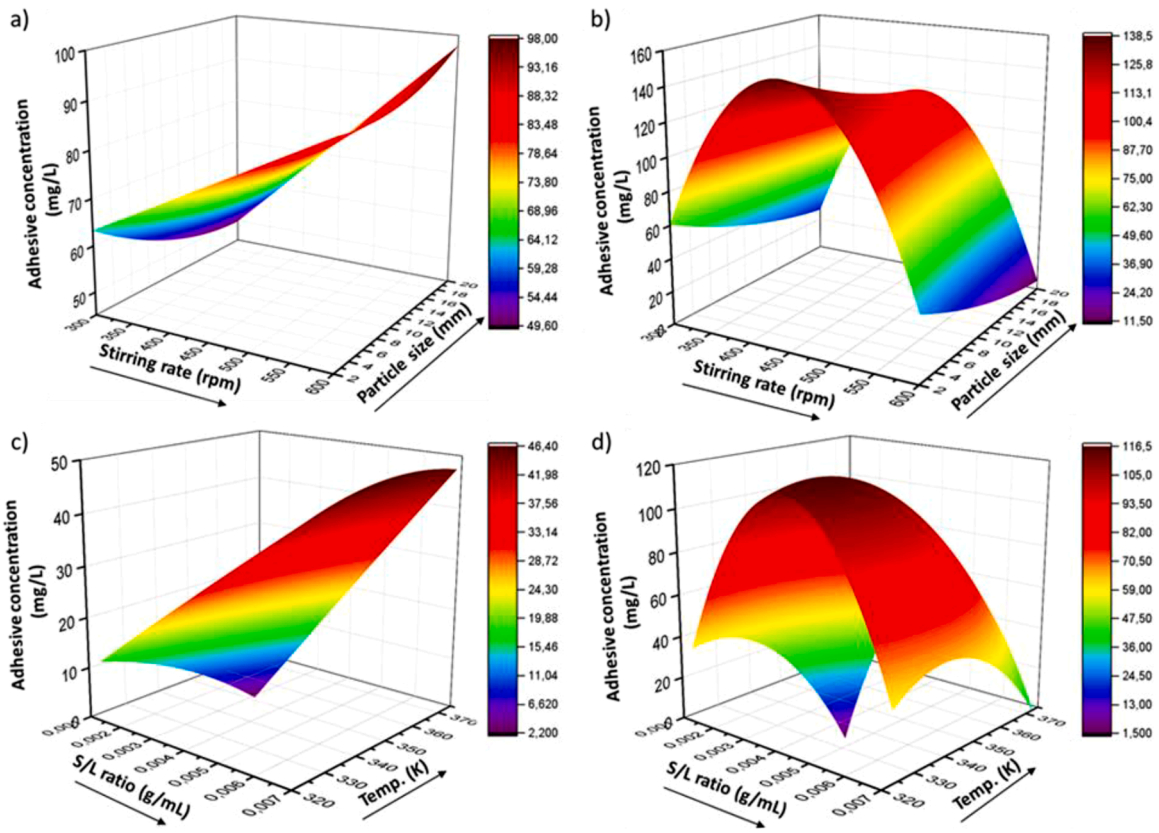

Fig. 3. Response surfaces of adhesive concentration (mg/L) as a function of a) stirring rate and particle size for sample B (PET based MFPF laminated with SB-PU adhesive); b) stirring rate and particle size for sample D (PE-based MFPF laminated with SB-PU adhesive); c) S/L ratio and temperature for ample D; d) S/L ratio and temperature for sample C (PE-based MFPF laminated with SF-PU adhesive).

$$Conc\left(\frac{mg}{L}\right)_D = 12.53425 + 1.4863 * x_1 + 1.9726 * x_2 + 5.12785 * x_3 - 3.31963 * x_4 - 3.40411 * x_1 * x_2 + 1.45205 * x_2 * x_3 - 3.27397 * x_3 * x_4 - 25.50685 * x_1^2 + 25.19521 * x_2^2 + 1.28425 * x_4^2 \quad (14)$$

Via these quadratic equations, based on the constant values, it is possible to evaluate which parameter or interaction of parameters has the most pronounced effect on the increase in adhesive concentration. For example, among all the process variables, the S/L ratio (x_3) makes the highest contribution in sample A (with a constant value 28.0337), followed by temperature (x_2), in terms of obtaining a higher adhesive concentration and thus faster delamination. Similarly, for Samples B and D, a higher adhesive dissolution is observed with increased temperature (x_2). On the other hand, the delamination of Sample C is influenced primarily by the stirring rate (x_1) and particle size (x_4). This may be due to the composition of Sample C, i.e., a PE-based MFPF laminated with SF-PU adhesive, which exhibits slower delamination kinetics as compared to other plastic compositions because the diffusivity through PE film and the solubility of SF-PU adhesives are lower. In terms of the interaction of parameters, temperature and S/L ratio interaction have the highest impact on increasing the adhesive concentration for all the MFPFs, even though their contribution is different for each sample, which originates mainly from the differences in the composition of MFPFs. Because the thickness and constituent polymer layers of each MFPF are different, their responses to the changes in experimental parameters differ. Furthermore, two types of adhesives (SB-PU and SF-PU) are used in the MFPF. Because the solubility levels of these adhesives differ, the dissolution of the adhesives during delamination is affected divergently by changing conditions. The relationship between the sample composition and the experimental parameters is visualized through the surface plots given in Fig. 3.

Although the interaction of stirring rate (x_1) and particle size (x_4) does not have a dominant effect on the delamination rate of MFPFs based on the quadratic equations, different MFPFs have diverse optimal values for these parameters. Therefore, Fig. 3a and 3b show the interaction effect of stirring rate and particle size on the delamination rate of Samples B (PET-based MFPF) and D (PE-based MFPF), respectively. According to the results, Sample D is affected more heavily by the change in stirring rate as compared to Sample B. For example, increasing the stirring rate from 300 rpm to 450 rpm results in more than a two-fold increase in the adhesive concentration during the delamination of Sample D. Because the delamination of MFPFs is triggered by the diffusion of the reagent through constituent polymer layers, it is expected to observe higher delamination rates at higher stirring rates due to increased diffusion. However, interestingly, a decrease in adhesive concentration in Sample D is observed at 450 rpm. This may be explained by the change in the flow regime. At higher stirring rates, a cyclonic type of flow may occur, which results in less turbulence in the flask (Rajavathsavai, Khapre, & Munshi, 2014). This may cause reduced interaction between the reagent and the MFPF, resulting in slower adhesive dissolution. On the other hand, the results show that the efficient delamination of Sample B can be obtained mainly at high stirring rates, e.g., 600 rpm. This may be due to the presence of a lacquer layer on Sample B. Although the diffusion of the reagent is limited at higher stirring rates, friction between the MFPFs is enhanced, which facilitates the removal of the coating layer (De Meester, Roosen, & Ügdüler, 2021). In terms of particle size, Sample B tends to delaminate more slowly at smaller particle sizes as compared to Sample D. This may be due to the presence of a coating layer on the surface of Sample B, which delays the diffusion of acid to the adhesive layer. However, neither sample shows a

Table 6
The optimal delamination conditions for each MFPF.

Sample	Temperature (°C)	Stirring rate (rpm)	S/L ratio(g/mL)	Particle size (mm)	Dissolved adhesive at 60 min (%)
A	100.00	600	0.0070	11.00	92.1
B	100.00	600	0.0057	20.00	90.5
C	75.07	497	0.0042	20.00	60.0
D	100.00	442	0.0070	2.00	52.1

significant response to changes in particle size. This also proves that the frontal diffusion of the reagent is a more profound factor in the delamination of MFPFs than lateral diffusion (through the sides of MFPFs), in which particle size would affect the delamination rate significantly. Furthermore, the cross-interaction of S/L ratio and temperature, which has the highest impact on adhesive concentration increase based on the quadratic equations, is shown in Fig. 3c and 3d for Samples D and C, respectively. As temperature is also a diffusion promoting factor, it is expected to observe higher delamination rates at increased temperatures. This has been confirmed for both samples. For example, for Sample D, the highest adhesive concentration (48 mg/L) was obtained at the highest tested temperature (100°C). Although Sample C has an optimal delamination temperature of 75°C, this may be due to the interaction effect between S/L ratio and temperature. This also shows that the S/L ratio has a more profound effect on the delamination rate of Sample C as compared to Sample D. This may originate from the differences in the chemical properties of the adhesives used in Samples C (SF-PU) and D (SB-PU). Because the solubility of SF-PU (0.73 mg/mL at 95°C) adhesive is substantially lower than the solubility of SB-PU adhesive (18 mg/mL at 95°C), lower S/L ratios are required for the MFPFs containing SF-PU adhesive.

Based on all these interactions between the experimental parameters (temperature, stirring rate, S/L ratio, and particle size), optimal delamination conditions were determined for each MFPF, under which the maximum adhesive concentration was obtained after 60 minutes of reaction between formic acid and each MFPF. The results are presented in Table 6.

As seen in Table 6, even under optimized conditions, different adhesive dissolution rates were obtained during the delamination process. For example, the adhesive dissolution % for PET-based MFPFs (Samples

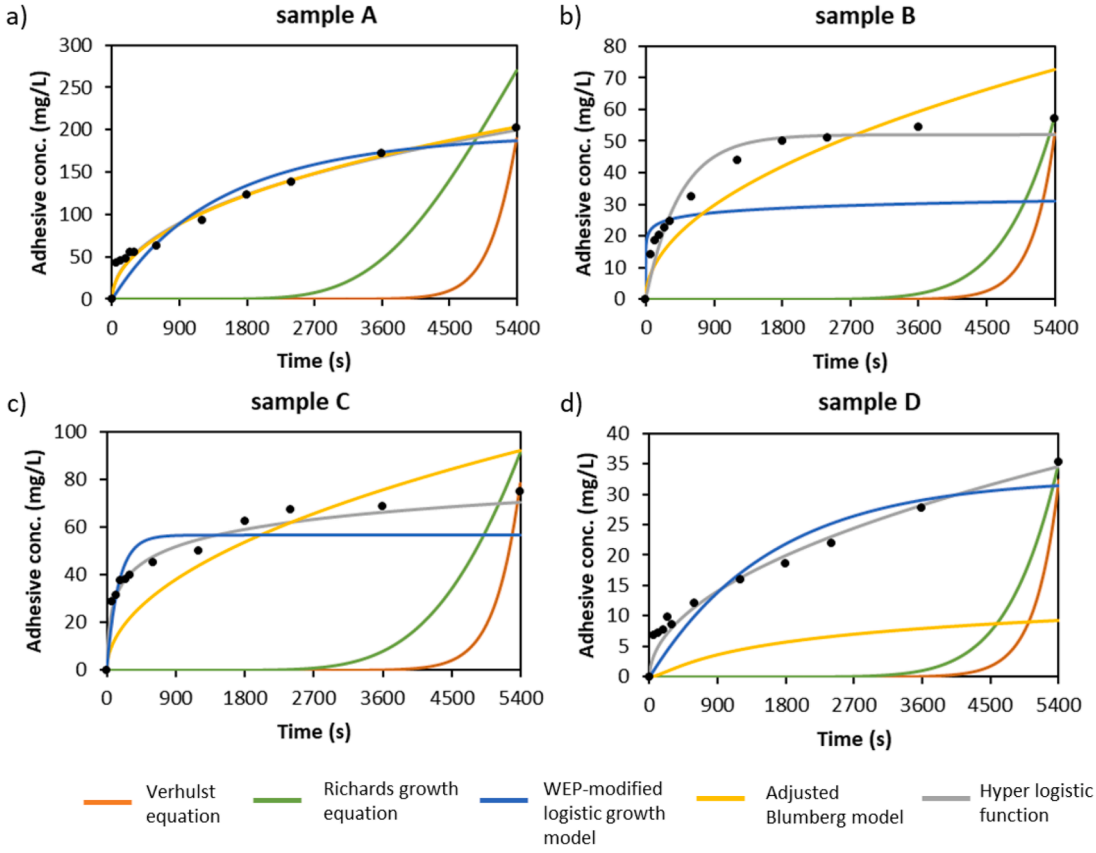

Fig. 4. Comparison between experimental data (exp.no: 8, at 87.5°C, 525 rpm, 0.0055 g/mL S/L ratio and 6.5 mm particle size) (shown as dots) and five kinetic models (shown as lines) describing the adhesive concentration (mg/L) during delamination as a function of time for a) sample A; b) sample B; c) sample C; d) sample D.

Table 7
The average results of the validation techniques (SSE, TIC, χ2, and HYBRID) for four MFPFs per tested kinetic model.

Kinetic model	Average				Standard deviation			
	SSE	TIC	χ^2	HYBRID	SSE	TIC	χ^2	HYBRID
Verhulst equation	6726.9	0.529	164.45	1494.9	6528.7	0.050	84.09	764.45
Richards growth equation	6164.4	0.522	158.26	1582.5	5707.3	0.049	76.39	763.89
Hyper-logistic Function	153.2	0.058	6.66	74.0	143.2	0.006	4.79	53.19
Adjusted Blumberg model	364.2	0.119	15.23	152.3	180.5	0.044	5.92	59.17
WEP-modified logistic growth model	300.6	0.085	12.26	122.6	266.5	0.011	8.33	83.26

Table 8
Conditions set in the Aspen Plus® simulations for delamination of sample A and corresponding heat and energy consumption in each step of the process flow at the acid evaporation ratio in the (final) flash unit (%).

	Acid evaporation ratio in the (final) flash unit (%)					Unit
	90%	92.5%	95%	97.5%	100%	
Plastic load	1000	1000	1000	1000	1000	kg/h
Adhesive load	34.74	34.74	34.74	34.74	34.74	mg/g
Temperature reactors	87.5	87.5	87.5	87.5	87.5	°C
Pressure	1.00	1.00	1.00	1.00	1.00	bar
Particle size	6.5	6.5	6.5	6.5	6.5	mm
S/L ratio	0.0055	0.0055	0.0055	0.0055	0.0055	g/mL
Total acid consumption	56.92	56.92	56.92	56.92	52.62	kg/h
Adhesive removal	95%	95%	95%	95%	95%	-
Lime consumption	121.03	121.03	121.03	121.03	121.03	kg/h
Plastic flash dryer						
Energy consumption: Heat	19.12	19.12	19.12	19.12	19.12	kWh
Neutralisator						
Energy release	-69.55	-69.55	-69.55	-69.55	-69.55	kWh
Net energy consumption: Heat	0	0	0	0	0	kWh
Pump heat cycle neutralization-flash						
Energy consumption pump: Electricity	0.33	0.33	0.33	0.33	0.33	kWh
Plastic mechanical dryer						
Energy consumption: Electricity	90	90	90	90	90	kWh
Plastic thermal dryer						
Energy consumption: Heat	168.44	168.44	168.44	168.44	168.44	kWh
Flash column						
Net heat consumption	4.98	4.83	4.67	4.52	1.70	MWh
Vacuum system (Compressor)						
Energy consumption: Electricity	6016.76	6184.05	6351.51	6519.69	7843.88	kWh
Pump bottom fraction flash						
Energy consumption: Electricity	0.82	0.68	0.52	0.34	0.00	kWh
Heat recovery for flash recycle						
Heat duty heater feed: Heat	0	0	0	0	0	kWh
Waste						
Salt (calcium formate)	74.39	74.39	74.39	74.39	74.39	kg/h
Feed incinerator	37.3	37.3	37.3	37.3	33.0	kg/h
Adhesive feed incinerator	33.0	33.0	33.0	33.0	33.0	kg/h
Water generated during neutralization	99.27	99.27	99.27	99.27	99.27	kg/h

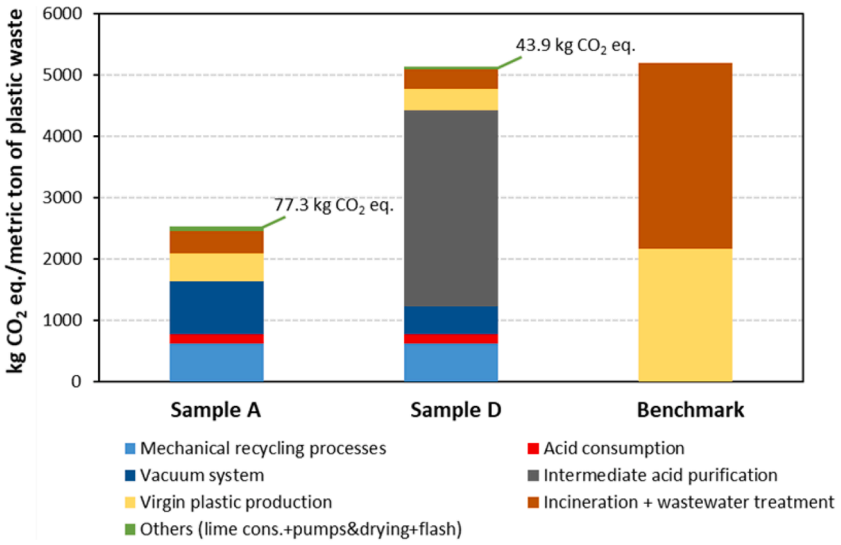

Fig. 5. GHG emission analysis of delamination process for samples A and D (expressed as kg CO_2-eq per metric ton of plastic film waste) in comparison to the benchmark (incineration + waste water treatment and virgin plastic production).

A and B) is much higher as compared to the PE-based MFPFs (Samples C and D). The compositional difference between the MFPFs affects the diffusion rate of the reagent; hence, different delamination rates are obtained.

3.2. Modeling of the delamination process

3.2.1. Best-fit kinetic model

In order to describe the delamination kinetics of various MFPFs for the simulation of the delamination process in Aspen Plus®, different kinetic models (the Verhulst equation, Richards growth equation, hyper logistic function, adjusted Blumberg model, and WEP-modified logistic growth model) that consider potential lag time due to the diffusion and also the saturation of the liquid medium were tested, as shown in Fig. 4.

An error analysis was also applied to the tested models by using various validation techniques (i.e., sum of square of errors (SSE), hybrid fractional error function (HYBRID), Theil's inequality coefficient (TIC), and nonlinear Chi-square test (χ^2)), and the average results of these

statistical tests are presented in Table A-1. The applied validation techniques also show that the hyper-logistic function is better able to describe the kinetics of the delamination under various experimental conditions than the other functions. On the other hand, both the Verhulst equation and the Richards growth equation result in TIC values above 0.3, indicating that these kinetic models are not suitable to describe the delamination kinetics.

As can be seen in Fig. 4 and Table 7, among the tested models, the experimental kinetic data fit best the hyper-logistic function model (gray line). Only Sample A showed similar fits to the adjusted Blumberg and hyper-logistic models (overlapping yellow and gray lines) under the conditions of Experiment 8, as seen in Figure 4, but the validation techniques clearly indicate that the hyper-logistic function model exhibits a better fit to the experimental data. By considering the hyper-logistic function from a theoretic perspective, it can be stated that this model describes the population dynamics or chemical kinetics in terms of a sigmoid-like curve that consists of three phases, namely a lag phase, a growth phase, and a saturation phase (Anguelov, Kyurkchiev, & Markov, 2018). As discussed in our previous study (Ügdüler et al., 2021), the delamination of MFPFs also occurs in three stages. Firstly, a period of acid diffusion through the polymer layers is observed (lag phase). Secondly, the diffused acid through the polymer layers begins to dissolve the adhesive. The dissolution of the adhesive increases gradually when more acid diffuses through the polymer layers (growth phase). Lastly, the adhesive concentration in the medium reaches a plateau, indicating that all adhesives existing between the polymer layers are dissolved and the constituent polymer layers are separated from one another (saturation phase). According to the hyper-logistic function, this overall process is described as given in Eq. (15):

$$\frac{d[PU_L]}{dt} = k_1 * [PU_L]^{k_2} * \left(1 - \frac{[PU_L]}{[PU_L]_{eq}}\right)^{k_3} \quad (15)$$

where $[PU_L]$ is the concentration of adhesive in the liquid (mg/L); $[PU_L]_{eq}$ is the maximal solubility of the adhesive in the liquid at the particular temperature (mg/L); and k_1, k_2, and k_3 are the rate constants. The modelled rate constants for each MFPF sample under each experimental condition (Table 5) are given in Appendix, Table A-2.

3.2.2. Energy consumption analysis

The recovery of the delaminated plastic films and acid medium was studied through Aspen Plus® simulations. In order to determine the effect of sample composition on medium recovery, the simulations were performed for both Samples A (PET-based MFPF laminated with SF-PU adhesive) and D (PE based MFPF laminated with SB-PU adhesive) at a capacity of 1000 kg/h. In the simulations, different acid evaporation ratios in the (final) flash unit (between 90% and 100%) were considered for both samples. For Sample A, the corresponding heat and energy consumption values in each process step at different acid evaporation ratios are given in Table 8. For Sample D, these values are shown in Table A-3.

The simulation indicates that the acid recovery is primarily responsible for the high energy consumption in the downstream component of the delamination process. This is mainly due to the low solubility of the adhesives in formic acid. In order to dissolve larger amounts of adhesives in the acid medium and thus increase the delamination rate, a large volume of acid is required. In order to prevent the supply of fresh acid each time, the acid medium was distilled and condensed prior to recirculation. In fact, the energy consumption of the acid recovery process was minimized through the optimization of temperature and pressure in the flash drum. In addition, the heat generated by the vacuum system was used to heat up the flash drum. For example, during the acid recovery process for Sample D, no extra energy was used for the flash drum, because the heat recovered from the vacuum system was sufficient to distill the entire amount of acid. Despite these process optimizations to minimize energy consumption, the use of large volumes of acids negatively affects the downstream process of delamination. Especially for Sample D, the intermediate acid purification process, which includes condensation of acid after each reactor (ten reactors in total) to increase the solubility of the adhesive, resulted in very high energy consumption (23,062 kW per 1 ton of MFPF), as shown in Table A-3. When the processes with different acid evaporation ratios (%) are compared, it is observed that the evaporation of more acid slightly increases the energy consumption, especially for the vacuum system. For example, to obtain a 90% acid evaporation ratio, the vacuum system consumes 6017 kWh energy, while this value increases to 7844 kWh to obtain 100% acid evaporation ratio. Because the acid that is not evaporated (e.g., 10% in the case of a 90% acid evaporation ratio) is sent back to the reactor, the total acid consumption does not change based on variations in the acid evaporation ratio. In general, the optimization of the downstream process based on the delamination kinetics of MFPF and also the solubility of adhesive plays an important role in minimizing energy consumption and thus increasing the economic and environmental benefits of the delamination process.

3.3. Life cycle assessment

A life cycle assessment (LCA) was performed for both Samples A (PET-based MFPF laminated with SF-PU adhesive) and D (PE based MFPF laminated with SB-PU adhesive) in order to investigate the effect of sample composition on the carbon footprint of the delamination process. Aspen Plus® simulations showed that differences in acid evaporation ratio (%) do not affect the energy consumption of the entire delamination process significantly; thus, the LCA calculations were performed by considering only the delamination process with a 95% acid evaporation ratio. The result has been expressed in terms of carbon dioxide equivalents (CO_2-eq) per metric ton of MFPF waste. As explained in Section 2.6, the washing of MFPF waste before the delamination process, the treatment of the waste water, and the extrusion of the delaminated plastic films after the delamination were also included in the LCA calculations. Based on these considerations, the greenhouse gas (GHG) emissions of each step during the recycling of both MFPFs and the benchmark (i.e., incineration with energy recovery and the production of virgin polymers) are given Fig. 5.

Fig. 5 shows that the net GHG emissions of the recycling process for 1 ton of Sample A (2523 kg CO2-eq) are less than half of the GHG emissions of the benchmark (5192 kg CO2-eq). This indicates that delamination with formic acid is a potentially environmentally beneficial process when recycling MFPFs with a composition similar to that of Sample A (PET-based MFPF). On the other hand, the net GHG emissions of the recycling process for 1 ton of Sample D (5130 kg CO2-eq) are almost equal to the GHG emissions of virgin plastic production and incineration. This is mainly due to the chemical composition of Sample D (PE-based MFPF), which results in slower delamination. In order to increase the kinetics of Sample D and also the solubility of the SF-PU adhesive in Sample D, its delamination process was optimized through, for example, intermediate acid purification steps. Even though higher adhesive removal yields (58%, Table A-3) would be obtained, these intermediate steps (3201 kg CO2-eq) affect the total carbon footprint of the process negatively. Therefore, the trade-off between more purification versus slower kinetics is very relevant to the upscaling of the delamination of MFPFs with compositions similar to that of Sample D. When the impacts of various delamination steps on the total carbon footprint of process are compared, the vacuum system (compressor) contributes most heavily to GHG emissions during the delamination of Sample A due to the recovery of large amount of acid. The GHG emissions of the vacuum system used in the process for Sample D were lower than those for Sample A because the heat recovered from the intermediate purification process for Sample D was sufficient to compensate for the energy consumption of the flash drum and the vacuum system. In general, the LCA shows that the type of adhesive and the multilayer sample composition are crucial to the delamination process in terms of carbon emissions as compared to incineration, which is the current state-of-the-art.

4. Conclusion

In this study, the optimal delamination conditions of various MFPFs in formic acid were investigated. Among the evaluated process variables (temperature, S/L ratio, stirring rate, and particle size), the combination of temperature and S/L ratio had the most pronounced effect on the delamination rate. In terms of sample composition, higher delamination rates were obtained for the PET-based MFPFs (>90%) as compared to the PE-based MFPFs (<60%) due to the faster diffusion of formic acid through PET films as compared to PE films. In addition, the presence of a coating layer on the MFPF surface causes lower delamination rates.

Aspen Plus® simulations on the PET- and PE-based MFPFs revealed that the delamination kinetics of the MFPF and dissolution rates of the adhesive are the determining factors in the energy consumption of the process. For the PE based MFPFs laminated with SF-PU adhesive, a larger amount of fresh acid is needed to increase the solubility of the adhesive and thus the delamination rate. Even though the process can be adjusted to recirculate the acid, the condensation of large amounts of acid causes high energy consumption. The lower solubility of SF-PU adhesive compared to SB-PU adhesive may be related to its synthesis route. The hardness of SF-PU is generally higher because no solvent is used during its synthesis, resulting in the limited growth of pores within the polymer structure. This affects the swelling ratio of the polymer negatively, thus decreasing its solubility. Therefore, PET-based MFPFs laminated with SB-PU adhesive have more potential in terms of scaling up their delamination process. Because different carboxylic acids will affect the solubility of the adhesives differently, the optimization of delamination should be performed based on the type of medium.

Finally, the LCA results show that the high energy consumption during the delamination process, especially due to the purification of large volumes of acids, strongly affects the GHG emissions of the entire process. If the MFPF has fast delamination kinetics and contains an adhesive with high solubility in the medium, e.g., PET-based MFPF laminated with SB-PU adhesive, the delamination process is very beneficial in terms of CO_2 emissions as compared to incineration. On the other hand, the LCA shows that the delamination of MFPFs with slow delamination kinetics, such as PE-based MFPF can hardly compete with the CO_2 emissions of incineration. This indicates that, even though there are many adhesive options in the market, chemical uniformity would be advantageous in terms of the recycling of MFPFs. In addition, improving the solubility capacity of the delamination medium, e.g., via the addition of certain reagents, would lower the volume of reagent necessary to dissolve adhesives, thus creating economic benefits. More generally, this study shows that process optimization, together with "design for delamination", is key to obtaining a competitive delamination process for various MFPFs in terms of both economic and environmental benefits.

CRediT Author Statement

Sibel Ügdüler: Conceptualization, Methodology, Investigation, Writing - Original Draft **Tobias De Somer:** Methodology, Investigation, Writing - Original Draft **Kevin M. Van Geem:** Writing - Review & Editing, Funding acquisition **Juray De Wilde:** Writing - Review & Editing **Martijn Roosen:** Methodology, Investigation, Writing - Review & Editing **Bram Deprez:** Methodology **Steven De Meester:** Conceptualization, Resources, Writing - Review & Editing, Supervision, Project administration, Funding acquisitionEqns 2–(6)

CRediT authorship contribution statement

Sibel Ügdüler: Conceptualization, Methodology, Investigation, Writing – original draft. **Tobias De Somer:** Methodology, Investigation, Writing – original draft. **Kevin M. Van Geem:** Writing – review & editing, Funding acquisition. **Juray De Wilde:** Writing – review & editing. **Martijn Roosen:** Methodology, Investigation, Writing – review & editing. **Bram Deprez:** Methodology. **Steven De Meester:** Conceptualization, Resources, Writing – review & editing, Supervision, Project administration, Funding acquisition.

Declaration of Competing Interest

The authors declare that they have no known competing financial interests or personal relationships that cdocould have appeared to influence the work reported in this paper.

Acknowledgements

We thank Siegwerk Druckfarben AG & Co KGaA for providing the multilayer samples. We thank also Prof. Kim Ragaert for the access to the polarized optical microscopy. This work has received support from the European Regional Development Fund (ERDF) via the PSYCHE project (Interreg France-Wallonie-Vlaanderen), with co-financing from the provinces of East-Flanders and West-Flanders. The authors are grateful for the financial support provided by the Catalisti-Moonshot project Multilayer granted by the Vlaams Agentschap Innoveren & Ondernemen (VLAIO). The research leading to these results has also received funding from the European Research Council (ERC) under the European Union's Horizon 2020 Programme (P8/2007–2013)/ERC grant agreement no. 818607 (OPTIMA). In addition, the authors would like to acknowledge the financial support received from the Fund for Scientific Research Flanders (FWO) for the project WASTE.

Appendix A. Appendix Title

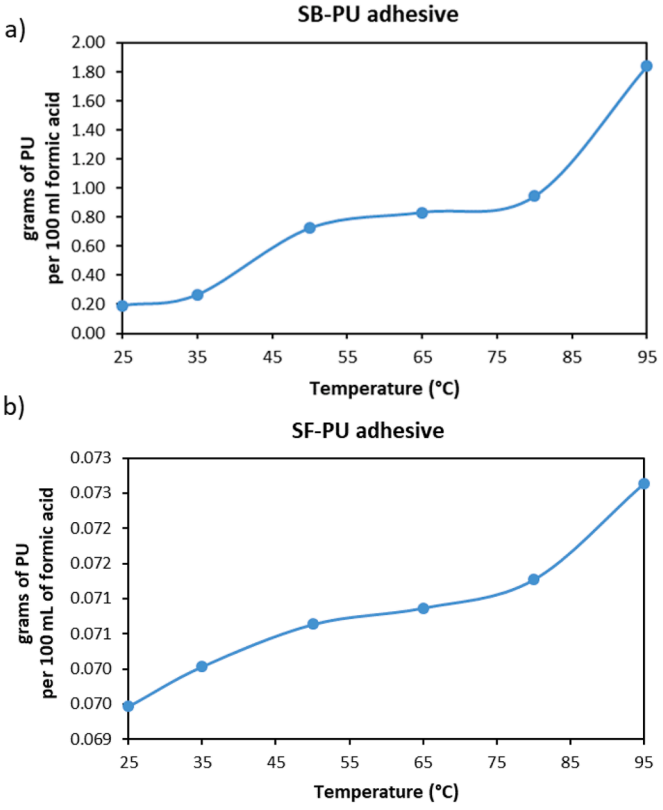

Fig. A-1. The solubility of a) SB-PU adhesive; b) SF-PU adhesive in formic acid in the temperature range between 25°C and 95°C.

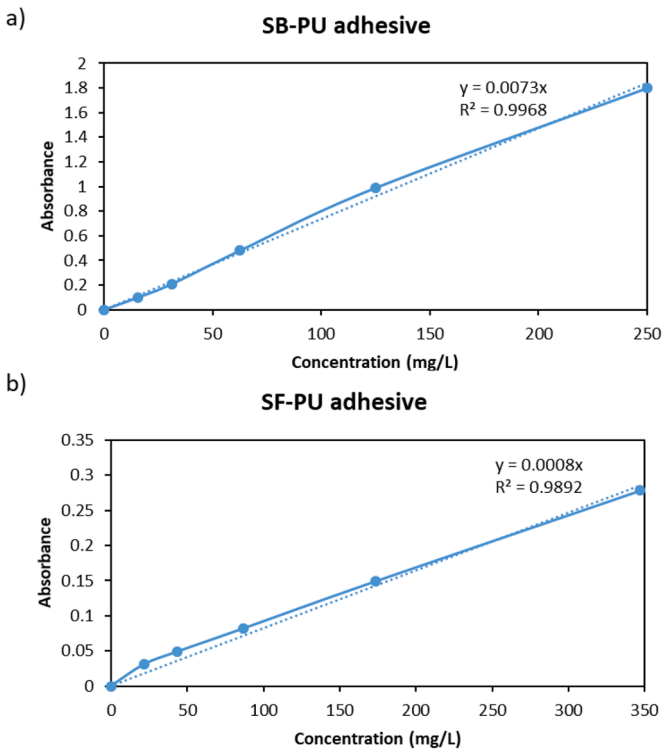

Fig. A-2. Calibration curves of a) SB-PU adhesive; b) SF-PU adhesive used to follow dissolution kinetics of adhesives in formic acid medium during delamination.

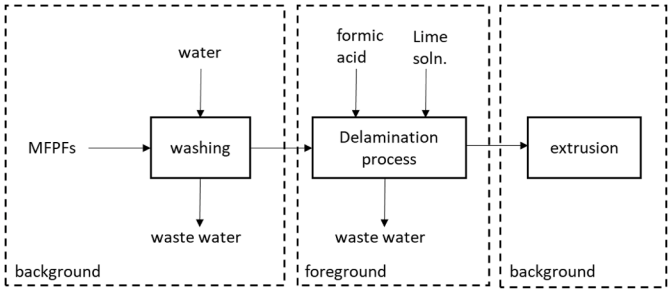

Fig. A-3. The foreground and background systems considered in the LCA.

Table A-1
The results of the validation techniques (SSE, TIC, χ2 and HYBRID) of four MFPFs separately per tested kinetic model.

	Kinetic model	Average				Standard deviation			
		SSE	TIC	χ^2	HYBRID	SSE	TIC	χ^2	HYBRID
Sample A	Verhulst equation	17,856.85	0.493	298.63	2714.82	20,271.07	0.072	184.20	1674.53
	Richards growth equation	15,864.65	0.455	279.00	2789.99	17,870.72	0.079	169.89	1698.87
	Hyper logistic Function	387.01	0.062	14.83	164.81	425.54	0.029	14.08	156.47
	Adjusted Blumberg model	544.55	0.081	18.60	185.95	537.30	0.040	14.08	140.85
	WEP-modified logistic growth model	727.15	0.088	26.39	263.86	900.50	0.040	18.69	186.85
Sample B	Verhulst equation	3062.47	0.522	124.71	1133.70	3891.18	0.091	93.70	851.81
	Richards growth equation	3002.35	0.510	122.86	1228.62	3829.17	0.091	92.85	928.51
	Hyper logistic Function	26.70	0.047	2.63	29.20	40.22	0.029	3.01	33.44
	Adjusted Blumberg model	191.80	0.085	10.68	106.78	379.37	0.044	13.80	138.03
	WEP-modified logistic growth model	83.69	0.066	5.85	58.54	154.38	0.035	6.25	62.50
Sample C	Verhulst equation	4626.16	0.613	163.27	1484.26	6820.39	0.062	118.68	1078.88
	Richards growth equation	4448.87	0.592	159.55	1595.52	6462.15	0.065	115.28	1152.80
	Hyper logistic Function	152.31	0.062	4.84	53.77	387.17	0.033	8.45	93.86
	Adjusted Blumberg model	544.64	0.192	23.14	231.42	802.57	0.159	18.08	180.76
	WEP-modified logistic growth model	324.70	0.096	10.27	102.74	783.35	0.042	15.96	159.60
Sample D	Verhulst equation	1362.39	0.488	71.18	647.10	3350.49	0.097	60.07	546.06
	Richards growth equation	1341.73	0.530	71.61	716.07	3141.91	0.178	58.70	586.97
	Hyper logistic Function	46.82	0.061	4.36	48.40	163.19	0.036	9.97	110.72
	Adjusted Blumberg model	175.72	0.121	8.49	84.90	756.29	0.163	15.05	150.46
	WEP-modified logistic growth model	67.04	0.087	6.54	65.37	133.06	0.035	6.78	67.79

Table A-2
The rate constant values used for fitting of the hyper logistic function to the experimental data of delamination kinetics of each MFPF under tested conditions.

	Sample A			Sample B			Sample C			Sample D		
Expno	k_1	k_2	k_3	k_1	k_2	k_3	k_1	k_2	k_3	k_1	k_2	k_3
1	0.087	-1.000	1.00E-10	0.014	-1.000	351.866	0.104	0.732	411.722	0.001	0.263	8.71419E-05
2	0.215	-0.715	1.00E-04	0.007	0.222	377.408	0.089	0.554	193.838	0.005	0.609	1282.001
3	2.753	1.041	292.974	0.006	-0.386	387.892	9.771	-1.000	133.321	0.047	-1.000	1148.447
4	0.030	0.223	20.867	0.002	0.195	3.75E-06	0.900	-0.277	106.989	0.035	-1.000	497.066
5	0.196	-1.000	3.135	0.173	-1.000	432.421	0.021	1.161	174.803	0.006	0.252	1664.977
6	0.012	0.406	2.372	0.216	-0.354	1014.372	0.134	0.287	136.868	0.024	-0.838	0.000
7	0.017	0.087	0.003	0.022	-0.144	1366.507	3.026	-1.000	400.390	0.007	0.322	4278.189
8	5.191	-1.000	1.579	0.425	-0.129	972.516	15.218	-1.000	42.855	0.133	-1.000	129.703
9	2.203	-1.000	21.708	118.500	1.116	4611.423	1.148	-1.000	113.553	0.006	0.650	3213.182
10	2.371	-1.000	23.883	0.017	0.600	1953.135	0.528	-0.509	289.410	1.247	-1.000	3099.101
11	2.948	-1.000	231.635	0.005	-0.451	269.336	0.008	-1.000	623.701	0.001	0.000	375.475
12	0.088	-0.778	1.00E-06	0.005	0.128	1.00E-04	0.155	0.509	357.292	0.010	0.558	5413.001
13	0.035	-1.000	1.00E-06	0.014	-0.790	4.595	21.287	-1.000	80.044	0.107	1.117	5817.599
14	0.048	-0.449	1.00E-06	0.006	-0.071	1.00E-04	2.479	1.261	228.747	0.451	-1.000	628.368
15	0.042	-0.453	2.24E-08	0.112	0.788	5603.534	3.611	-1.000	913.899	0.001	0.463	0.000
16	0.251	-0.713	1.00E-06	0.224	0.836	2201.810	7.839	1.369	554.434	0.103	-0.831	0.000
17	0.176	-1.000	23.504	0.133	0.595	4479.972	0.125	-1.000	104.238	0.002	0.360	0.0000001
18	0.033	0.539	22.380	1.152	-1.000	198.273	1.111	-1.000	48.241	0.021	-1.000	1.33043E-07
19	0.217	0.016	18.383	0.082	-0.435	790.405	0.444	-1.000	200.552	0.002	-0.229	0.000
20	0.068	-0.066	5.715	0.076	-0.272	942.593	1.387	-1.000	72.733	0.047	-0.992	183.977
21	0.026	-0.198	23.715	0.004	0.203	251.443	0.201	-1.000	638.193	0.002	0.161	1033.420
22	0.772	-0.799	0.000	0.029	-0.212	3256.460	41.100	1.185	1020.019	0.009	0.342	0.000
23	0.038	-0.168	0.054	2.164	-1.000	484.836	38.500	1.275	813.594	0.020	-0.553	0.000
24	0.074	0.280	20.055	0.067	0.372	1658.719	1.500	-0.346	214.782	0.267	-1.000	1830.749
25	0.118	1.106	160.032	0.017	0.317	1304.139	3.310	-0.981	80.721	0.042	0.702	13,909.906
26	1.719	-1.000	0.789	0.001	0.053	1.00E-04	3.773	-1.000	160.181	0.462	-1.000	1230.148
27	0.011	0.364	47.495	0.018	0.432	880.206	4.421	-1.000	16.648	0.028	0.159	1172.935
28	0.125	-0.863	0.000	0.017	0.181	691.309	0.268	0.925	266.816	2.187	-1.000	4107.598
29	0.023	0.084	4.465	0.006	0.564	420.532	0.181	0.510	118.903	0.091	-1.000	1662.218
30	2.546	-1.000	2.114	0.808	-1.000	509.220	0.155	0.349	95.771	0.205	-1.000	620.082

Table A-3
The conditions used in the Aspen Plus® simulations for delamination of sample D and the corresponding heat and energy consumption in each step of the process flow at different acid evaporation ratios (%).

	Acid evaporation ratio in the (final) flash unit (%)					Unit
	90%	92.5%	95%	97.5%	100%	
Plastic load	1000	1000	1000	1000	1000	kg/h
Adhesive load	43.42	43.42	43.42	43.42	43.42	mg/g
Temperature reactors	87.5	87.5	87.5	87.5	87.5	°C
Pressure	1.00	1.00	1.00	1.00	1.00	bar
Particle size	6.5	6.5	6.5	6.5	6.5	mm
S/L ratio	0.0055	0.0055	0.0055	0.0055	0.0055	g/mL
Total acid consumption	55.73	55.73	55.73	55.73	52.63	kg/h
Adhesive removal	53	54	55	56	58	%
Lime consumption	121.03	121.03	121.03	121.03	121.03	kg/h
Plastic flash dryer						
Energy consumption: Heat	19.12	19.12	19.12	19.12	19.12	kWh
Neutralisator						
Energy release	-69.55	-69.55	-69.55	-69.55	-69.55	kWh
Net energy consumption: Heat	0	0	0	0	0	kWh
Pump heat cycle neutralization-flash						
Energy consumption pump: Electricity	0.33	0.33	0.33	0.33	0.33	kWh
Plastic mechanical dryer						
Energy consumption: Electricity	90	90	90	90	90	kWh
Plastic thermal dryer						
Energy consumption: Heat	168.44	168.44	168.44	168.44	168.44	kWh
Flash column						
Net heat consumption	0	0	0	0	0	MWh
Vacuum system (Compressor)						
Energy consumption: Electricity	3299.8	3299.8	3299.8	3299.8	3299.8	kWh
Pump bottom fraction flash						
Energy consumption: Electricity	1.37	1.37	1.37	1.37	1.37	kWh
Heat recovery for flash recycle						
Heat duty heater feed: Heat	-555.5	-582.0	-608.6	-635.0		kWh
Intermediate acid purification (reactors 1–10)						
Net heat consumption: Heat	125.54	125.63	125.71	125.78	125.78	kWh
Energy consumption Vacuum: Electricity	23,061.83	23,061.76	23,061.69	23,061.63	23,061.63	kWh
Recovery Bottom flash						
Net heat consumption: Heat	0	0	0	0	0	kWh
Energy consumption Vacuum: Electricity	173.32	178.16	183.03	188.02	188.02	kWh

(*continued on next page*)

Table A-3 (*continued*)

	Acid evaporation ratio in the (final) flash unit (%)					Unit
	90%	92.5%	95%	97.5%	100%	
Energy consumption pump: Electricity	0.09	0.07	0.05	0.02	0.02	kWh
Waste						
Salt (calcium formate)	74.39	74.39	74.39	74.39	74.39	kg/h
Feed incinerator	27.0	27.0	27.0	27.0	27.0	kg/h
Adhesive feed incinerator	23.9	23.9	23.9	23.9	23.9	kg/h
Water generated during neutralization	99.27	99.27	99.27	99.27	99.27	kg/h

Table A-4
Carbon footprint values of each step of the delamination process at 95% acid evaporation ratio.

Process	Value		Unit
	Sample A	Sample D	
Mechanical recycling processes			
$FeCl_3$	0.73	0.73	kg CO_2-eq/ton waste
NaOH	1.94	1.94	kg CO_2-eq/ton waste
Polyelectrolyte	0.29	0.29	kg CO_2-eq/ton waste
Washing water	0.03	0.03	kg CO_2-eq/ ton waste
Float-sink	0.01	0.01	kg CO_2-eq/ton waste
Electricity for the whole mechanical recycling process	174.13	174.13	kWh/ton waste
Natural gas	15.13	15.13	MJ/ton waste
Incineration of non-plastic substances e.g. *paper*	500.26	500.26	kg CO_2-eq/ton waste
Avoided electricity due to energy recovery during mechanical recycling	-42.54	-42.54	kWh/ton waste
Avoided heat	-30.83	-30.83	MJ/ton waste
Acid consumption	181.88	178.09	kg CO_2-eq/ton waste
Lime consumption	38.55	38.57	kg CO_2-eq/ton waste
Water used in lime solution	0.01	0.01	kg CO_2-eq/ton waste
Salt (calcium formate)	197.95	197.95	kg CO_2-eq/ton waste
Feed incinerator	99.22	71.77	kg CO_2-eq/ton waste
Adhesive feed incinerator	87.81	63.52	kg CO_2-eq/ton waste
Water generated during neutralization	59.41	59.41	kg CO_2-eq/ton waste
Plastic flash dryer	0.16	0	kWh/ton waste
Flash drum	39.73	0.000011	kWh/ton waste
Plastic thermal dryer	1.43	0	kWh/ton waste
Plastic mechanical dryer	15.26	15.26	kWh/ton waste
Pump heat cycle neutralization-flash	0.05	0.05	kWh/ton waste
Vacuum system	1077.22	559.66	kWh/ton waste
Pump bottom fraction flash	0.09	0.23	kWh/ton waste
Intermediate acid purification	0	3942.31	kWh/ton waste

References

Addev Materials, (2021). Surface treatment [WWW Document]. URL https://www.addevmaterials.eu/converting/surface-treatment (accessed 6.29.21).

Anguelov, R., Kyurkchiev, N., Markov, S., 2018. Some properties of the Blumberg's hyper-log-logistic curve. BIOMATH 7, 1–8. https://doi.org/10.11145/j.biomath.2018.07.317.

Bawn, C.E.H., Freeman, R.F.J., Kamaliddin, A.R., 1950. High polymer solutins. Trans. Faraday Soc. 46, 677–684.

Beer, A., 1852. Bestimmung der absorption des rothen lichts in farbigen flüssigkeiten (Determination of the absorption of red light in colored liquids). Ann. der Phys. und Chemie 86, 78–88.

Bercea, M., Eckelt, J., Wolf, B.A., 2009. Vapor pressures of polymer solutions and the modeling of their composition dependence. Ind. Eng. Chem. Res. 48, 4603–4606. https://doi.org/10.1021/ie801965h.

Bing, C. (2012). Method for separating and recycling aluminum and plastics. CN101797574 B.

CEFLEX, (2021). End of Life challenges [WWW Document]. URL https://ceflex.eu/flexible-packaging-in-europe/(accessed 9.16.21).

Civancik-Uslu, D., Nhu, T.T., Van Gorp, B., Kresovic, U., Larrain, M., Billen, P., Ragaert, K., De Meester, S., Dewulf, J., Huysveld, S., 2021. Moving from linear to circular household plastic packaging in Belgium: prospective life cycle assessment of mechanical and thermochemical recycling. Resour. Conserv. Recycl. 171, 1–12. https://doi.org/10.1016/j.resconrec.2021.105633.

Civancik-Uslu, D., Puig, R., Hauschild, M., Fullana-i-Palmer, P., 2019. Life cycle assessment of carrier bags and development of a littering indicator. Sci. Total Environ. 685, 621–630. https://doi.org/10.1016/j.scitotenv.2019.05.372.

Coperion, (2020). How to make high-quality plastic compounds out of packaging. URL: https://www.coperion.com/cn/newsmedia/newsletter/2021/plastics-in-focus-edition-012021/apk-relies-on-coperion-zsk-extruder-technologyAccess date: 9.16.21.

De Meester, S., Roosen, Martijn, & Ügdüler, S. (2021). A method to deink plastic material. PCT/EP2021/058652.

European Commission, (2018). New waste rules will make EU global front-runner in waste management and recycling.

Hamilton, J.A., 1999. Transport of fatty acids across membranes by the diffusion mechanism. Prostaglandins Leukot. Essent. Fat. Acids 60, 291–297. https://doi.org/10.1016/S0952-3278(99)80002-7.

Horodytska, O., Valdés, F.J., Fullana, A., 2018. Plastic flexible films waste management – a state of art review. Waste Manag 77, 413–425. https://doi.org/10.1016/J.WASMAN.2018.04.023.

Herbold, (2016). Information sheet 49: mechanical Dryer/Centrifugal Washer.URL: https://herboldusa.com/images/documents/info_sheet_49_mechanical_dryer.pdfAccess date: 9.11.21.

Huang, C.-K., & Shao, C.-H. (2002). Separating method for recycling foil-laminated material. US20040129372A1.

Ji, L.Q., 2013. Analysis of a modified logistic model for describing the growth of durable customer goods in China. Math. Comput. Appl. 18, 30–37. https://doi.org/10.3390/mca18010030.

Kaiser, K., Schmid, M., Schlummer, M., 2018. Recycling of polymer-based multilayer packaging: a review. Recycling 3, 1–26. https://doi.org/10.3390/recycling3010001.

Kippenhahn, R., Knauf, U., Luck, T., Mäurer, A., Schlummer, M., & Wolz, G. (2003). Method for separating and recovering target polymers and their additives from a material containing polymers. EP1311599A1.

Kulkarni, A.K., Daneshvarhosseini, S., Yoshida, H., 2011. Effective recovery of pure aluminum from waste composite laminates by sub- and super-critical water. J. Supercrit. Fluids 55, 992–997. https://doi.org/10.1016/j.supflu.2010.09.007.

Larrain, M., Van Passel, S., Thomassen, G., Van Gorp, B., Nhu, T.T., Huysveld, S., Van Geem, K.M., De Meester, S., Billen, P., 2021. Techno-economic assessment of mechanical recycling of challenging post-consumer plastic packaging waste. Resour. Conserv. Recycl. 170, 105607 https://doi.org/10.1016/j.resconrec.2021.105607 https://doi.org/.

Lindner, W. (2000). Method of separating polyolefinic synthetic mixtures. WO2000077082.

Lovis, F., Seibt, H., & Kernbaum, S. (2015). Method and apparatus for recycling packaging material. WO2015169801A1.

Lynch, C. J., & Nauman, E. B. (1994). Polymer recycling by selective dissolution. US5278282A.

Massura, A. C., Marçal De Souza, E. A., & Crochemore, G. B. (2002). Process for separation of multilayered films used for packagings. WO2003104315A1.

Mukhopadhyay, A. (2001). Process of de-lamination of multi-layer laminated packaging industrial refuse. US20040054018A1.
Mumladze, T., Yousef, S., Tatariants, M., Kriukiene, R., Makarevicius, V., Lukošiute, S.I., Bendikiene, R., Denafas, G., 2018. Sustainable approach to recycling of multilayer flexible packaging using switchable hydrophilicity solvents. Green Chem 20, 3604–3618. https://doi.org/10.1039/c8gc01062e.
National Lime Association, 2000. Fact sheet on using lime for acid neutralization. Arlington. https://www.lime.org/documents/publications/free_downloads/acid-neut-final-2000.pdfAccessdate:7.29.21.
Niaounakis, M., 2019. Solvent- and/or chemical agent-based separation. In: Payne, E. (Ed.), Recycling of Flexible Plastic Packaging. Matthew Deans, Oxford, United Kingdom, pp. 211–264.
Noda, I., Higo, Y., Ueno, N., Fujimoto, T., 1984. Semidilute region for linear polymers in good solvents. Macromolecules 17, 1055–1059. https://doi.org/10.1021/ma00135a013.
Nowofol, (2021). Polyolefin films [WWW Document]. URL https://www.nowofol.com/en/polyolefin-films/(accessed 6.29.21).
Patel, K. M., Patel, M. M., & Vaviya, M. H. (2016). Process for recovering low-density polyethylene from flexible packaging material. WO2015159301A3.
Plastemart, (2020). MOPE films for lamination & recyclability [WWW Document]. URL http://www.plastemart.com/press-release-plastics-industry/mope-films-for-lamination-recyclability/7074 (accessed 6.29.21).
Rajavathsavai, D., Khapre, A., Munshi, B., 2014. Study of mixing behavior of cstr using cfd. Brazilian J. Chem. Eng. 31, 119–129. https://doi.org/10.1590/S0104-66322014000100012.
Rathbone, S.J., Haynes, C.A., Blanch, H.W., Prausnitz, J.M., 1990. Thermodynamic properties of dilute aqueous polymer solutions from low-angle laser-light-scattering measurements. Macromolecules 23, 3944–3947. https://doi.org/10.1021/ma00219a013.
Sadeghi, R., Shahebrahimi, Y., 2011. Vapor pressure osmometry determination of solvent activities of different aqueous and nonaqueous polymer solutions at 318.15 K. J. Chem. Eng. Data 56, 2946–2954. https://doi.org/10.1021/je200176t.
Sakurada, I., Nakajima, A., Fujiwara, H., 1959. Vapor pressures of polymer solutions. II. Vapor pressure of the poly(vinyl alcohol)-water system. J. Polym. Sci. 35, 497–505. https://doi.org/10.1002/pol.1959.1203512916.
Schulze, M. (2018). Separation fluid, method and apparatus for recycling multilayer material using a metal passivation agent. GB2574260A.
Schyns, Z.O.G., Shaver, M.P., 2020. Mechanical recycling of packaging plastics: a review. Macromol. Rapid Commun. 42, 1–27. https://doi.org/10.1002/marc.202000415.
Sheehan, C.J., Bisio, A.L., 1966. Polymer/solvent interaction parameters. Rubber Chem. Technol 149–192.
Sobek, J., Polak, J., & Hajek, M. (2015). Method for separating composite packaging materials. WO2017108014A1.
Sweilam, N.H., Khader, M.M., Mahdy, A.M.S., 2012. Numerical studies for solving fractional-order logistic equation. Int. J. Pure Appl. Math. 78.
Thome, R. D., Kraus, S., & Schubert, J. (1993). Process for treating or working up composite and plastic materials. EP0644230A1.
Tiseo, I. (2021). Flexible packaging production volume in 2017 and 2022.
Tsoularis, A., Wallace, J., 2002. Analysis of logistic growth models. Math. Biosci. 179, 21–55. https://doi.org/10.3159/08-RA-004.1.
Ügdüler, S., De Somer, T., Van Geem, K.M., Roosen, M., Kulawig, A., Leineweber, R., De Meester, S., 2021. Towards a better understanding of delamination of multilayer flexible packaging films by carboxylic acids. ChemSusChem cssc 14, 4198-421. https://doi.org/10.1002/cssc.202002877, 202002877.
Ügdüler, S., Van Geem, K.M., Denolf, R., Roosen, M., Mys, N., Ragaert, K., De Meester, S., 2020. Towards closed-loop recycling of multilayer and coloured PET plastic waste by alkaline hydrolysis. Green Chem 22, 5376–5394. https://doi.org/10.1039/D0GC00894J.
Xianghui, D. (2007). Plastic-aluminum separating agent and plastic-aluminum separating method. CN100535039C.
Zawadiak, J., 2017. Tetra pak recycling – current trends and new developments. Am. J. Chem. Eng. 5, 37–42. https://doi.org/10.11648/j.ajche.20170503.12.
Zeide, B., 1993. Analysis of growth equations. For. Sci. 39, 594–616. https://doi.org/10.1093/forestscience/39.3.594.
Zhou, S., Wu, L., Xiong, M., He, Q., Chen, G., 2004. Dispersion and UV-VIS properties of nanoparticles in coatings. J. Dispers. Sci. Technol. 25, 417–433. https://doi.org/10.1081/DIS-200025688.